Steady-state and dynamic simulation of a grinding mill using grind curves

J. D. le Roux[a,*], A. Steinboeck[b], A. Kugi[c], I. K. Craig[a]

[a] *Department of Electrical, Electronic and Computer Engineering, University of Pretoria, Pretoria, South Africa.*
[b] *Automation and Control Institute, Vienna University of Technology, Gußhausstraße 27-29, 1040 Vienna, Austria*
[c] *Christian Doppler Laboratory for Model-Based Control in the Steel Industry, Automation and Control Institute, Vienna University of Technology, Gußhausstraße 27-29, 1040 Vienna, Austria*

Abstract

A dynamic non-linear model was fitted to the grind curve data of an industrial semi-autogenous grinding (SAG) mill by means of a step-wise procedure. Grind curves give the steady-state values of the performance variables throughput, power draw, and grind in terms of the mill filling and critical mill speed. The grind curves indicate the operable region of the grinding mill. An analysis and dynamic simulation of the model show that the model captures the main dynamics of the grinding mill. Further simulations demonstrate that the model represents the full range of steady-state conditions defined by the grind curves. In other words, the dynamic model is quantitatively accurate as it settles at the correct steady-state for the operable region of the grinding mill. Therefore, the model is suitable as a simulator to test and develop optimizing control strategies for global operating conditions rather than only for local operating conditions.

Keywords: comminution, grinding mill, grind curves, modelling, process control, plant-wide control, simulation

1. Introduction

Since grinding mills have a significant impact on the final economic performance of a mineral processing plant (McIvor and Finch, 1991; Sosa-Blanco et al., 2000), it is important to operate them at the point which will optimize the economic performance of the plant (Cramer, 2008; **?**). Grinding mill processes are difficult to control as the control strategy has to contend with time-varying ore characteristics, non-linearities, constraints on manipulated and controlled variables, and a lack of quality measurements (Wei and Craig, 2009).

The general control objectives are to maximize the process throughput, maintain the grind at a set point that enables optimal downstream recovery, and use as little power as possible. Throughput, grind and power draw are also the three main variables which affect the economic performance of the mill (Le Roux and Craig, 2019). A comprehensive or plant-wide control strategy for a grinding mill comprises a regulatory, supervisory, and optimization layer. The regulatory layer stabilizes the plant, the supervisory layer maintains the economic controlled variables at set point by sending set points to the regulatory layer, and the optimization layer determines the set points of the economic controlled variables (Skogestad, 2004). In this paper, throughput is defined as the rate at which content discharges from the mill. Although throughput equals feed-rate at steady-state, they are not necessarily equal during dynamic changes. In addition, the grind of the mill is defined as the fraction of material in the discharge smaller than a specification size.

Grind curves provide the steady-state relationship between the throughput, grind, and power to the volumetric filling and rotational speed of the grinding mill (Powell and Mainza, 2006). As the volumetric filling

*Corresponding author. Address: Department of Electrical, Electronic, and Computer Engineering, University of Pretoria, Pretoria, South Africa. Tel.: +27 12 420 2201; Fax: +27 12 362 5000. E-mail: derik.leroux@up.ac.za

and rotational speed of the grinding mill varies, the mill goes through a non-linear dynamic response. Therefore, the grind curves can be regarded as quazi-steady-state or approximately steady-state representations of the feasible operating conditions of the mill.

Grind curves assist in finding the set points of the economic controlled variables that optimize the economic performance of the mill (Le Roux and Craig, 2019). By way of example, Craig et al. (1992) developed a throughput-optimizer based on the grind curves of an industrial single-stage closed semi-autogenous grinding (SAG) mill circuit. It was observed that the maximum throughput occurred at a slightly lower mill filling than where maximum power is drawn. A heuristic power-peak-seeking algorithm was used to determine at which milling filling maximum power is drawn, and then operate at a slightly lower mill filling to maximize throughput. The controller was also required to maintain an acceptable product particle size as chosen by operating staff. Similarly, Steyn and Sandrock (2013) aimed to optimize grind for an industrial single-stage closed autogenous grinding (AG) mill circuit. Grind curves were developed in terms of mill filling and mill inlet water and indicated an approximate region where optimal grind occurs. A supervisory model predictive controller was used to maintain the plant at the optimal operating condition given by the grind curves. For both examples above, economic performance assessments showed that the control strategies significantly increased the profitability of the plant.

Before implementing an optimizing controller on an industrial plant, it is preferable to test the control strategy in simulation (Sbarbaro and del Villar, 2010). To evaluate a plant-wide control strategy in simulation a model is required which describes the dynamics of the process controlled by the regulatory and supervisory layers, as well as the range of steady-state conditions controlled by the optimization layer (Le Roux and Craig, 2019).

A common approach to model industrial grinding mills is to derive linear time-invariant models from step-test data. These type of models are common to design controllers for grinding mills (Craig and MacLeod, 1996; Pomerleau et al., 2000; Chen et al., 2007), even though the model parameters are subject to considerable uncertainty (Craig and MacLeod, 1995). Since the models represent a linearization of the system at a specific operating condition, they provide a locally limited description of the system dynamics. In addition, because the mineralogy of the ore changes over time (Tungpalan et al., 2015), the models require frequent state and parameter updates (Olivier and Craig, 2013).

Fundamental phenomenological models are more suited to describe the non-linear dynamic response of a grinding mill (Valery and Morrell, 1995; Salazar et al., 2009; Hinde and Kalala, 2009). These models are often used to develop supervisory control strategies such as model predictive control for grinding mills (Apelt and Thornhill, 2009; Salazar et al., 2014). However, these fundamental models generally contain large parameter sets which are difficult to estimate and update from the scarce measurements available on industrial plants (Le Roux et al., 2017). The dynamic model presented by Le Roux et al. (2013) uses a significantly reduced parameter set while producing qualitatively accurate model responses, i.e., the model captures the correct direction of controlled variables for movements in manipulated variables but does not accurately represent the full range of feasible steady-state conditions. Although the model is not suitable for the physical design of a grinding mill, the model serves as a good basis for controller development (Coetzee et al., 2010; Le Roux and Craig, 2013; Le Roux et al., 2016).

A significant challenge when modelling grinding mills is to separate the characteristics of the ore from the characteristics of the grinding environment (Powell and Morrison, 2007). This is especially true for models of the breakage rate as the models have to represent the full range of operating conditions given by the grind curves. The mill filling and rotational speed have a large impact on the breakage rates in the mill (Van der Westhuizen and Powell, 2006; Morrell, 2004).

The novel contribution of this article is a quantitatively accurate dynamic simulation model of a grinding mill, i.e., the model describes the short-term dynamics and the steady-state behaviour as represented by grind curves. The rotational speed of the mill is included as a manipulated variable in the simulation model. The purpose of the simulation model is to serve as a platform to evaluate and develop hierarchical control strategies over a wide range of operating conditions. Therefore, the model not only allows evaluation of controllers in the regulatory and supervisory layers at various operating conditions, but also the interplay between the optimization layer and the supervisory layer over the full range of feasible steady-state operating conditions (Le Roux and Craig, 2019). The article presents a step-wise procedure to fit the model to grind

curve data measured at industrial mills, such that the model can be used by practitioners to characterize their own plant and evaluate their control strategy in simulation.

The paper is organized as follows: Section 2 describes the process and the process model. Section 3 discusses grind curve data from industrial plants. Section 4 shows a step-wise procedure to fit the model to measured grind curve data. Section 5 presents the dynamic and steady-state characteristics of the model in simulation and Section 6 gives a brief conclusion.

2. Process

This section provides a description of the SAG mill shown in Fig. 1. The model of the SAG mill is discussed and presented in state-space form.

2.1. Process Description

The variables for the SAG mill illustrated in Fig. 1 are listed in Table 1. The mill receives three streams: mined ore (u_o) (t/h), water (u_w) (m^3/h), and steel balls (u_b) (t/h). The mill charge is a mixture of grinding media and slurry. Grinding media refers to the steel balls and rocks which break the ore, and slurry refers to the mixture of solids and water. The fraction of the mill filled with charge is denoted by J_T.

The mill is rotated along its longitudinal axis by a motor. The charge in the mill is lifted by the inner liners on the walls of the mill to a certain height from where it cascades down. The cascading motion of the charge causes the ore to break through impact breakage, abrasion, and attrition. The rotational speed

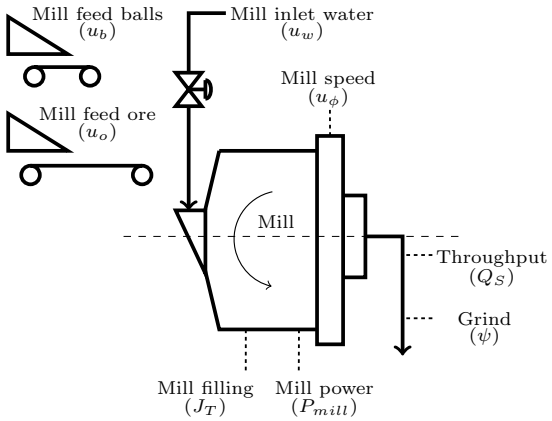

Figure 1: A semi-autogenous (SAG) mill.

Table 1: Description of comminution circuit variables.

Variable	Unit	Description
J_T	[-]	Fraction of mill volume filled with charge
P_{mill}	[kW]	Power draw
Q_F	[m^3/h]	Fines discharge flow-rate
Q_S	[m^3/h]	Solids discharge flow-rate
Q_W	[m^3/h]	Water discharge flow-rate
ρ_Q	[t/m^3]	Slurry density
ψ	[-]	Grind (volume fraction of particles in discharge < 150 μm)
u_b	[t/h]	Feed-rate of steel balls
u_o	[t/h]	Feed-rate of ore
u_w	[m^3/h]	Flow-rate of feed water
u_ϕ	[-]	Fraction of critical mill speed

of the mill is generally expressed as a fraction of the critical mill speed (u_ϕ), which is the rotational speed where the centrifugal acceleration of a particle at the mill shell equals the gravitational acceleration. The power draw (P_{mill}) (kW) of the motor turning the mill is an indicator of the kinetic and potential energy imparted to the charge.

The ground ore in the mill mixes with water to create a slurry. The density of the slurry is given by ρ_Q (t/m^3). The slurry is discharged through an end-discharge grate which limits the particle size of the discharged slurry. Ore too large to pass through the end-discharge grate are referred to as *rocks* and must be broken further. All ore small enough to pass through the end-discharge grate are referred to as *solids*. The flow-rate of solids and water discharging from the mill is given by Q_S and Q_W (m^3/h) respectively. Therefore, Q_S and Q_W represent the volumetric throughput of ore and water through the mill respectively.

The aim of the milling circuit is to grind the ore to below a specification size, e.g., 150 μm. The mill grind (ψ) is the volume fraction of material in the discharge of the mill below the specification size. The broken ore below the specification size are referred to as *fines*. The flow-rate of fines discharging from the mill is given by Q_F (m^3/h). Note, whereas solids refer to all ore small enough to discharge from the mill, fines refer to the portion of solids smaller than the specification size. Therefore, solids are a combination of fine ore and *coarse* ore, where coarse ore refers to the portion of solids larger than the specification size.

2.2. Dynamic Process Model

The SAG mill in Fig. 1 is modelled with the continuous time phenomenological non-linear population balance model of Le Roux et al. (2013). This simulation model is used in a variety of grinding mill control studies (Coetzee et al., 2010; Olivier and Craig, 2013; Le Roux et al., 2016; Aguila-Camacho et al., 2017; Wakefield et al., 2018). A brief overview of the model is given below. The model nomenclature is shown in Table 2.

Table 2: Parameter values. (Dimensionless parameters are shown without units.)

Parameter	Unit	Description
α_f	[-]	Volume fraction of fines in the feed ore
α_r	[-]	Volume fraction of rocks in the feed ore
δ_s	[-]	Power parameter for volume fraction of solids in the slurry
δ_v	[-]	Power parameter for volume of mill filled
d_q	[h^{-1}]	Discharge rate constant
ε_0	[-]	Maximum volume fraction of solids in the slurry at zero slurry flow
φ_N	[-]	Rheology normalization factor
$J_{TP_{max}}$	[-]	Fraction of mill volume filled at maximum power draw
K_{fp}	[kWh/t]	Fines production factor
K_{rc}	[kWh/t]	Rock consumption factor
P_{max}	[kW]	Maximum mill power draw
ρ_o	[t/m^3]	Density of ore
ρ_w	[t/m^3]	Density of water
v_{mill}	[m^3]	Mill volume
x_b	[m^3]	Volumetric filling of balls in mill

2.2.1. Population Balance

The population volume balance model describes four states: water (x_w), solids (x_s), rocks (x_r), and fines (x_f) (m^3):

$$\dot{x}_w = u_w - Q_W \tag{1a}$$

$$\dot{x}_s = (1-\alpha_r)\frac{u_o}{\rho_o} - Q_S + Q_{RC} \tag{1b}$$

$$\dot{x}_r = \alpha_r \frac{u_o}{\rho_o} - Q_{RC} \tag{1c}$$

$$\dot{x}_f = \alpha_f \frac{u_o}{\rho_o} - Q_F + Q_{FP}, \tag{1d}$$

where α_f and α_r represent the fraction of fines and rocks in u_o respectively, ρ_o ($\mathrm{t/m}^3$) is the ore density, Q_{RC} (m^3/h) is a rock consumption term that indicates the volumetric rate of rocks broken into solids, and Q_{FP} (m^3/h) is a fines production term that indicates the volumetric rate of ore broken into fines.

Although there are various ways to describe the consumption of steel balls in the mill (Apelt et al., 2002; Salazar et al., 2009; Le Roux et al., 2013), a constant ball volume (x_b) (m^3) is assumed for the purposes of this study. In practice operators often assume a linear proportionality between the total mass of ore milled and the consumption rate of steel balls. Based on this assumption, u_b is set at a ratio of u_o to maintain x_b constant (Gupta and Yan, 2006; Le Roux and Craig, 2019).

The fraction of the mill filled with charge (J_T) is given by:

$$J_T = \frac{x_w + x_s + x_r + x_b}{v_{mill}}, \tag{2}$$

where v_{mill} (m^3) is the total volume of the mill. It is assumed the void filling fraction is one.

The slurry density (ρ_Q) is defined as:

$$\rho_Q = \frac{\rho_w x_w + \rho_o x_s}{x_w + x_s} \tag{3}$$

where $\rho_w = 1$ $\mathrm{t/m}^3$ is the density of water.

The total discharge slurry mass flow-rate can be expressed as $M_T = M_S + M_W$ (t/h), where M_S and M_W are the total solids and water mass flow-rates respectively. Similarly, the total discharge slurry volumetric flow-rate can be expressed as $Q_T = Q_S + Q_W$ (m^3/h), where $Q_S = \frac{M_S}{\rho_o}$ and $Q_W = \frac{M_W}{\rho_w}$. Therefore, $Q_T = \frac{M_T}{\rho_Q} = \frac{M_S}{\rho_o} + \frac{M_W}{\rho_w}$. If there is 75% solids by mass in the slurry, then: $M_S = 0.75 M_T$ and $M_W = (1-0.75)M_T$. Therefore, the slurry density in (3) can also be expressed as:

$$\frac{1}{\rho_Q} = \frac{0.75}{\rho_o} + \frac{0.25}{\rho_w}. \tag{4}$$

2.2.2. Power

The mill power draw (P_{mill}) is modelled as:

$$P_{mill}\left(J_T, u_\phi\right) = \left(1 - \delta_v \left(\frac{J_T}{J_{TP_{max}}(u_\phi)} - 1\right)^2 - \delta_s \left(\frac{\varphi}{\varphi_N} - 1\right)^2\right) P_{max}(u_\phi), \tag{5}$$

where δ_v is the power change parameter for volume of mill filled, δ_s is the power change parameter for the volume fraction of solids in the slurry, φ is the rheology factor, and φ_N is a normalization factor. For $\varphi = \varphi_N$, P_{mill} reaches a maximum in terms of the volume fraction of solids in the slurry. $P_{max}(u_\phi) = \sum_k c_k^{(J_T)} u_\phi^k$ (kW) is the maximum mill power draw parametrized as a polynomial function of u_ϕ with coefficients contained in $\mathbf{c}^{(J_T)}$. $J_{TP_{max}}(u_\phi) = \sum_k c_k^{(P_{max})} u_\phi^k$ is the fraction of the mill filled at maximum power draw and is parametrized as a polynomial function of u_ϕ with coefficients contained in $\mathbf{c}^{(P_{max})}$.

The rheology factor φ is an empirically defined function that incorporates the effect of the fluidity and density of the slurry on the performance of the mill:

$$\varphi = \begin{cases} \sqrt{1 - \left(\varepsilon_0^{-1} - 1\right) \frac{x_s}{x_w}} & ; \quad \frac{x_s}{x_w} \leq \left(\varepsilon_0^{-1} - 1\right)^{-1} \\ 0 & ; \quad \frac{x_s}{x_w} > \left(\varepsilon_0^{-1} - 1\right)^{-1} \end{cases} \tag{6}$$

where $\varepsilon_0 = 0.6$ is the maximum fraction of solids by volume of slurry at zero slurry flow (Song et al., 2008). A rheology factor of one corresponds to $\frac{x_s}{x_w} = 0$ indicating the slurry consists only of water. A rheology factor of zero corresponds to $\frac{x_s}{x_w} = 1.5$ indicating the slurry is a non-flowing mud.

2.2.3. Breakage

The rock consumption (Q_{RC}) and fines production (Q_{FP}) are defined as:

$$Q_{RC} = \frac{P_{mill}\left(J_T, u_\phi\right)}{\rho_o K_{rc}\left(J_T, u_\phi\right)} \tag{7a}$$

$$Q_{FP} = \frac{P_{mill}\left(J_T, u_\phi\right)}{\rho_o K_{fp}\left(J_T, u_\phi\right)}. \tag{7b}$$

$K_{rc}\left(J_T, u_\phi\right)$ (kWh/t) is the rock consumption factor and indicates the energy required per tonne of rocks broken. $K_{fp}\left(J_T, u_\phi\right)$ (kWh/t) is the fines production factor and indicates the energy required per tonne of fines produced. The general formulation of the breakage equations is similar to the cumulative breakage rates expressions of Amestica et al. (1996) and Hinde and Kalala (2009).

The grind of the mill (ψ) is defined as:

$$\psi = \frac{x_f}{x_s} = \frac{Q_F}{Q_S}. \tag{8}$$

2.2.4. Discharge

The mill discharge flow-rates are defined as:

$$Q_W = d_q x_w \varphi \left(\frac{x_w}{x_s + x_w}\right) \tag{9a}$$

$$Q_S = d_q x_w \varphi \left(\frac{x_s}{x_s + x_w}\right) \tag{9b}$$

$$Q_F = d_q x_w \varphi \left(\frac{x_f}{x_s + x_w}\right), \tag{9c}$$

where d_q (1/h) is the discharge rate constant. Parameter d_q is used as a fitting parameter to account for different discharge grate designs (Latchireddi and Morrell, 2003a,b) and is representative of the pressure or driving force applied to the slurry to discharge from the mill. The discharge rate constant is multiplied with x_w in (9) as the main contributor to the driving force and with φ to consider the effect of x_s. The terms in brackets in (9) provide the fraction of water, solids or fines that can discharge from the mill through the end-discharge grate.

2.3. State-Space Representation

The model can be represented in state-space form as:

$$\begin{aligned} \tfrac{d}{dt}\mathbf{x}(t) &= \mathbf{f}\left(t, \mathbf{x}, \mathbf{u}, \mathbf{p}_1, \mathbf{p}_2, K_{rc}, K_{fp}, d_q\right) \\ \mathbf{y}(t) &= \mathbf{h}\left(t, \mathbf{x}, \mathbf{u}, \mathbf{p}_1, \mathbf{p}_2, K_{rc}, K_{fp}, d_q\right), \end{aligned} \tag{10}$$

where the states are $\mathbf{x} = \left[x_w, x_s, x_r, x_f\right]^T$, the manipulated variables are $\mathbf{u} = \left[u_w, u_o, u_\phi\right]^T$, and the measurable system outputs are $\mathbf{y} = [J_T, P_{mill}, Q_S, \psi]^T$. Function $\mathbf{f}(\cdot)$ is given by (1) and function $\mathbf{h}(\cdot)$ by (2), (5), (9b), and (8).

The set of known parameters in (10) are $\mathbf{p}_1 = \left[\alpha_f, \alpha_r, \varepsilon_0, \rho_o, v_{mill}, x_b\right]^T$. It is assumed that an on-line analysers measures α_f and α_r. It is also assumed that plant operators have a general estimate of x_b from regular sampling campaigns.

The mill power P_{mill} in (5) depends on the parametrization of $P_{max}(u_\phi)$ and $J_{T_{Pmax}}(u_\phi)$ as polynomial functions of the mill speed u_ϕ. The unknown parameters for P_{mill} are $\mathbf{p}_2 = \left[\delta_s, \delta_v, \varphi_{P_{max}}, \mathbf{c}^{(J_T)^T}, \mathbf{c}^{(P_{max})^T}\right]^T$.

The other unknown parameters are the ore breakage rates K_{rc} and K_{fp}, and the discharge rate constant d_q. An initial state $\mathbf{x}(t=0) = \mathbf{x}^*$ is required to simulate (10) using an appropriate numerical integration routine.

3. Grind Curves

Grind curves show the steady-state responses of P_{mill}, Q_S, and ψ as functions of J_T and u_ϕ. The term *grind curves* was introduced by Powell and Mainza (2006) (see also Van der Westhuizen and Powell (2006) and Powell et al. (2009)) to describe these well-known relationships in the mineral processing industry (Craig et al., 1992; Powell et al., 2001).

Powell and Mainza (2006) discuss the basic tools required to determine grind curves and illustrate the method for a pilot mill and an industrial SAG mill. This method is applied by Van der Westhuizen and Powell (2006) to an open circuit SAG mill to obtain a comprehensive set of grind curves. Similar grind curves for a variety of other mills are documented by Powell et al. (2011). Powell et al. (2009) discuss practical calibration issues to measure the grind curves and provide general guidelines on how to fit grind curves to measured data. Grind curves tend to change as the hardness and size distribution of the ore varies. A significant change in the general shape and position of the grind curves will usually indicate that a new type of ore is being processed (Viklund et al., 2006; Powell et al., 2009).

The grind curves measured by Van der Westhuizen and Powell (2006) are shown in Fig. 2. The commonly observed phenomenon responsible for the characteristic parabolic shape of the curves in terms of J_T is described by Van der Westhuizen and Powell (2006) and Le Roux and Craig (2019). In the case of Van der Westhuizen and Powell (2006), it is clear that the peaks of Q_S and P_{mill} do not coincide in terms of J_T, the curve shapes are dramatically changed by u_ϕ, the peak values change according to changes in u_ϕ, Q_S increases as u_ϕ increases, and ψ reduces as u_ϕ increases. An optimising controller has to balance these competing interactions to control a grinding mill.

Table 3 gives the parabolic expressions of the grind curves in Fig. 2, the location of their peaks, and the valid ranges of $J_T \in \left[\underline{J_T}, \overline{J_T}\right]$. The ranges of J_T ensure that the grinding mill does not enter infeasible operating conditions, e.g., for $u_\phi = \{0.6; 0.65\}$ in Fig. 2 the throughput Q_S approaches 0 m^3/h as J_T increases.

4. Parameter Fitting

The aim of this section is to describe a step-wise procedure to obtain the unknown model parameters in (10) from grind curve data so that the model produces both the dynamics and steady-state response of the grinding mill. This section is organized as follows:

- Section 4.1 discusses the initial data, assumptions, and the known parameters $\mathbf{p}_1$.
- Section 4.2 describes the parameter estimation of the unknown parameters $\mathbf{p}_2$ for P_{mill} in (5).
- Section 4.3 parametrizes the unknown breakage rates K_{rc} and K_{fp} in (7) in terms of J_T and u_ϕ.
- Section 4.4 establishes the unknown discharge rate constant d_q in (9) and an initial condition $\mathbf{x}^*$ for (10).

4.1. Data set

The procedure is illustrated with the data of Van der Westhuizen and Powell (2006) but can also be applied to similar data sets. The data of Van der Westhuizen and Powell (2006) is valuable in the open literature as it reports a wide range of u_ϕ and J_T whereas most other reports of grind curves are limited to a single value of u_ϕ.

The grind curves of Van der Westhuizen and Powell (2006) were obtained for an industrial open-circuit SAG mill of size $v_{mill} = 208$ m^3 (diameter: 7.8 m, length: 4.35 m) by running the mill to steady-state for a range of J_T between 0.2 and 0.45 and a range of u_ϕ between 0.60 and 0.75. The following conditions were

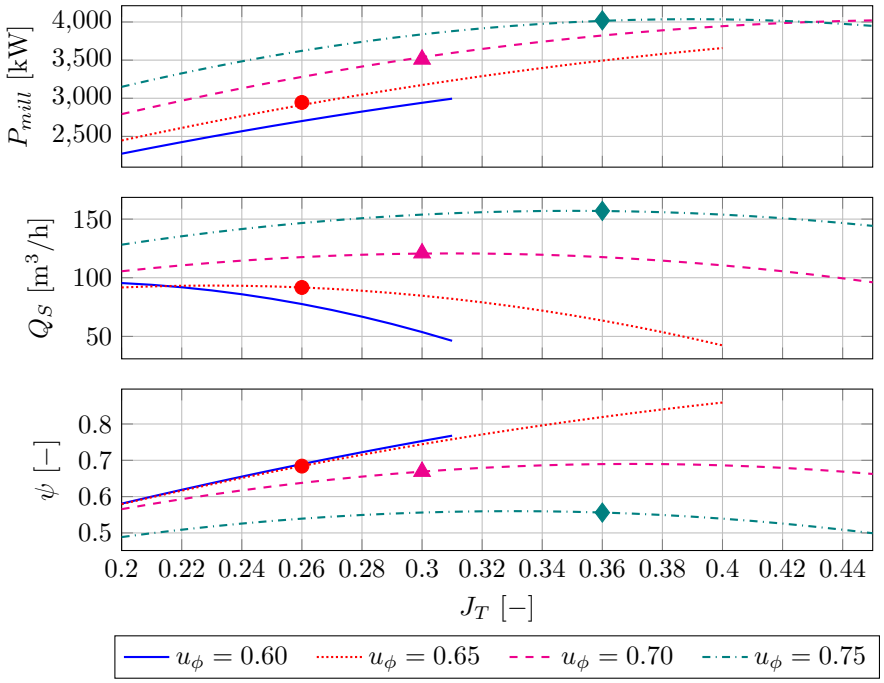

Figure 2: Grind curves for an open circuit SAG mill reproduced from Van der Westhuizen and Powell (2006). The range of J_T is limited for $u_\phi = 0.60$ and $u_\phi = 0.65$ as indicated in Table 3. (The three operating conditions in Table 4 are indicated as follows: Condition 1 - ○, Condition 2 - △, Condition 3 - ◇.)

Table 3: Grind curve polynomials $Y_{\square i}(J_T)$ as defined in (11) and their respective peak values (Van der Westhuizen and Powell, 2006). († indicates peaks extrapolated outside J_T range limits where $\underline{J_T}$ is the minimum and $\overline{J_T}$ is the maximum.)

Variable	i	u_ϕ	Polynomial	Peak	Range: $\left[\underline{J_T},\ \overline{J_T}\right]$
$Y_{P_{mill_i}}(J_T)$ [kW]	1	0.60	$(-11.5J_T^2 + 12.4J_T + 0.249) \times 10^3$	$Y_{P_{mill_1}}(0.54^\dagger) = 3600$	(0.2, 0.31)
	2	0.65	$(-12.1J_T^2 + 13.3J_T + 0.266) \times 10^3$	$Y_{P_{mill_2}}(0.55^\dagger) = 3930$	(0.2, 0.40)
	3	0.70	$(-17.0J_T^2 + 15.9J_T + 0.282) \times 10^3$	$Y_{P_{mill_3}}(0.47^\dagger) = 4030$	(0.2, 0.45)
	4	0.75	$(-24.6J_T^2 + 19.2J_T + 0.299) \times 10^3$	$Y_{P_{mill_4}}(0.39) = 4040$	(0.2, 0.45)
$Y_{Q_{S_i}}(J_T)$ [m^3/h]	1	0.60	$(-2.98J_T^2 + 1.07J_T) \times 10^3$	$Y_{Q_{S_1}}(0.18^\dagger) = 96.7$	(0.2, 0.31)
	2	0.65	$(-1.76J_T^2 + 0.812J_T) \times 10^3$	$Y_{Q_{S_2}}(0.23) = 93.3$	(0.2, 0.40)
	3	0.70	$(-1.26J_T^2 + 0.779J_T) \times 10^3$	$Y_{Q_{S_3}}(0.31) = 121$	(0.2, 0.45)
	4	0.75	$(-1.28J_T^2 + 0.897J_T) \times 10^3$	$Y_{Q_{S_4}}(0.35) = 157$	(0.2, 0.45)
$Y_{\psi_i}(J_T)$ [-]	1	0.60	$-2.27J_T^2 + 2.86J_T + 0.1$	$Y_{\psi_1}(0.63^\dagger) = 1.00$	(0.2, 0.31)
	2	0.65	$-2.50J_T^2 + 2.90J_T + 0.1$	$Y_{\psi_2}(0.58^\dagger) = 0.94$	(0.2, 0.40)
	3	0.70	$-4.31J_T^2 + 3.19J_T + 0.1$	$Y_{\psi_3}(0.37) = 0.69$	(0.2, 0.45)
	4	0.75	$-4.22J_T^2 + 2.79J_T + 0.1$	$Y_{\psi_4}(0.33) = 0.56$	(0.2, 0.45)

kept approximately constant during operation of the mill:

- Ball filling: $x_b = 0.079 v_{mill} = 16.4$ m^3.
- Ore density: $\rho_o = 2.7$ t/m^3.
- Slurry density: $\rho_Q = 1.9$ t/m^3.

As mentioned previously, plant operators do not measure the ball filling x_b on-line and only have a general estimate from sampling campaigns. The assumption of a constant ball filling is not restrictive as grind curves retain their parabolic shape for variations in the ball filling (Powell et al., 2009).

To maintain ρ_Q constant, u_w is controlled as a ratio of u_o. Therefore, ρ_Q remains at approximately 1.9 t/m^3 for all steady-state conditions given by the grind curves. Since a slurry density of $\rho_Q = 1.9$ t/m^3 corresponds to 75% solids by mass in the slurry, the ratio is $\beta_{ws} = \frac{Q_W}{Q_S} = \frac{(1-0.75)\rho_o}{0.75\rho_w} = 0.9$ (see (4)). Note, this ratio is valid at steady-state, but not during dynamic changes. (Although not considered in this study, the dimensionality of the grind curves can be extended by evaluating the response of P_{mill}, Q_S and ψ to changes in u_w (Steyn and Sandrock, 2013).)

Van der Westhuizen and Powell (2006) do not provide any dynamic data or ore feed data. The following assumptions are made regarding the input to the mill at steady-state:

- $u_o = \rho_o Q_S$: The feed-rate of ore into the mill equals the flow of ore exiting the mill.
- $u_w = Q_W$: The flow-rate of water into the mill equals the flow of water exiting the mill.
- The feed size distribution is $(\alpha_f, \alpha_r) = (0.1, 0.5)$. (This is not a restrictive assumption. The feed size distribution values can be updated given periodic sample measurements, or by measurements from an on-line instrument.)

Given the data above, the set of known parameters are:

$$\mathbf{p}_1 = \left[\alpha_f, \alpha_r, \varepsilon_0, \rho_o, v_{mill}, x_b\right]^T = [0.1,\ 0.5,\ 0.6,\ 2.7 \text{ t/m}^3,\ 208 \text{ m}^3,\ 16.4 \text{ m}^3]^T.$$

The curves in Fig. 2 are second order polynomials in terms of J_T for fixed values of u_ϕ:

$$Y_{\square i}(J_T) = \sum_{k=0}^{2} c_k J_T^k, \tag{11}$$

where $i = 1, \ldots, 4$ correspond to $u_{\phi_i} = \{0.6; 0.65; 0.7; 0.75\}$, c_k are constants, and $\square$ is a place holder for P_{mill}, Q_S, and ψ.

4.2. Mill Power Draw

The mill power draw model in (5) is fitted to the data in Table 3. The set of unknown parameters are given by $\mathbf{p}_2$. The following information can be gleaned from the available data described in Section 4.1:

- $\beta_{ws} = \frac{x_w}{x_s} = 0.9$ for all steady-state conditions since a controller maintains ρ_Q approximately constant. Therefore, $\varphi = 0.509$ from (6). Since no further information is available regarding the change in mill power with respect to a change in the fraction of solids in the slurry, it is assumed that $\varphi_N = 0.509$.
- Since the grind curves relate J_T to P_{mill}, it is possible to estimate δ_v in (5) from available data. However, since $\varphi = \varphi_N = 0.509$ at steady-state, the term associated with δ_s in (5) is zero for the steady-state conditions represented by the grind curves. Therefore, unless further information is available to relate ρ_Q to P_{mill} (see Steyn and Sandrock (2013)), it is not possible to estimate δ_s independently. Similar to Le Roux et al. (2013) and Coetzee et al. (2010), it is assumed in this case that $\delta_s = \delta_v$.

- As seen from Table 3, as u_ϕ increases, peak power is achieved for different values of J_T. The functions $J_{TPmax}(u_\phi)$ and $P_{max}(u_\phi)$ are parametrized as quadratic functions of u_ϕ.

The remaining unknown parameters are estimated as follows:

$$\min_{\left(\delta_s, \mathbf{c}^{(J_T)}, \mathbf{c}^{(P_{max})}\right)} \sum_{i=1}^{4} \int_{\underline{J_{Ti}}}^{\overline{J_{Ti}}} \left\| \frac{Y_{P_{mill_i}}(J_T) - P_{mill}(J_T, u_{\phi_i}, \mathbf{p}_2)}{\max(Y_{P_{mill_i}})} \right\|_2 dJ_T. \tag{12}$$

The result of this minimization is

- $\delta_s = \delta_v = 0.928$
- $J_{TP_{max}}(u_\phi) = -7.52u_\phi^2 + 9.06u_\phi - 2.18$
- $P_{max}(u_\phi) = (-2.70u_\phi^2 + 3.92u_\phi - 1.02) \times 10^4$ [kW].

Based on the estimated parameters, the comparison between $P_{mill}(J_T, u_\phi)$ in (5) and $Y_{P_{mill_i}}(J_T)$ in (11) is shown in Fig. 3. The normalized root mean squared error (NRMSE) is 6.10%.

4.3. Breakage Rates

The breakage rates K_{rc} and K_{fp} in (7) do not stay constant for changes in J_T and u_ϕ. The breakage rates can be back-calculated in terms of the grind curve variables in (11) by setting (1c) and (1d) equal to zero for steady-state where $u_o = \rho_o Q_S$. The result is:

$$K^*_{rc_i}(J_T) = \frac{Y_{P_{mill_i}}(J_T)}{\rho_o \alpha_r Y_{Q_{S_i}}(J_T)} \tag{13a}$$

$$K^*_{fp_i}(J_T) = \frac{Y_{P_{mill_i}}(J_T)}{\rho_o \left(Y_{\psi_i}(J_T) - \alpha_f\right) Y_{Q_{S_i}}(J_T)}, \tag{13b}$$

where $K^*_{\sigma_i}$ indicates a back-calculated value, $i = 1, \ldots, 4$ indicates the four different mill speeds $u_\phi = \{0.6; 0.65; 0.7; 0.75\}$, and $\sigma \in \{rc, fp\}$. Note, the ranges of J_T indicated in Table 3 should be obeyed,

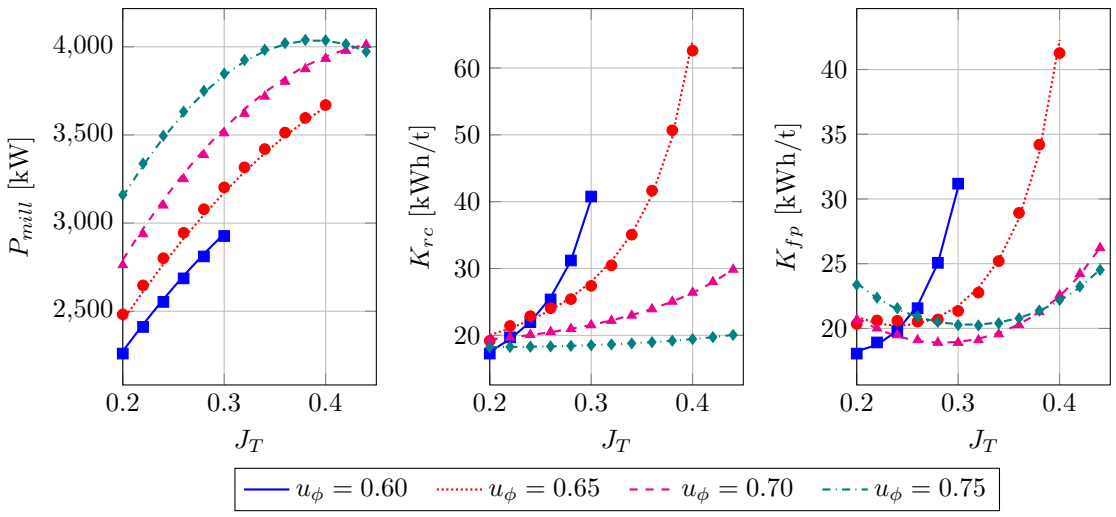

Figure 3: Left: Fit of $P_{mill}(J_T, u_\phi)$ model (data markers) to grind curves $Y_{P_{mill_i}}$ (lines). Centre: Fit of model of $K_{rc}(J_T, u_\phi)$ (data markers) to back-calculated values of $K^*_{rc_i}(J_T)$ (lines). Right: Fit of model of $K_{fp}(J_T, u_\phi)$ (data markers) to back-calculated values of $K^*_{fp_i}(J_T)$ (lines).

otherwise Q_S will approach zero at high J_T and low u_ϕ. Eq. (13) describes the breakage rates as functions of J_T for fixed values of u_ϕ. However, for simulation purposes it is also necessary to express the breakage rates as functions of u_ϕ. Therefore, the breakage rates are approximated as:

$$K_\sigma(J_T, u_\phi) = \sum_{n=0}^{N} \sum_{m=0}^{M} c_{m,n} u_\phi^m J_T^n, \tag{14}$$

where the coefficients $c_{m,n}$ are estimated by minimising the error between (13) and (14):

$$\min_{c_{m,n}} \sum_{i=1}^{4} \int_{\underline{J_{Ti}}}^{\overline{J_{Ti}}} \left\| \frac{K^*_{\sigma_i}(J_T) - K_\sigma(J_T, u_{\phi_i})}{\max\left(K^*_{\sigma_i}\right)} \right\|_2 dJ_T. \tag{15}$$

Eq. (15) is solved using the downhill simplex method after Nelder and Mead (1965). This is a well-known heuristic algorithm for multidimensional unconstrained non-linear optimization without derivatives. The result for $M = N = 3$ is:

$$\begin{aligned}
K_{rc}(J_T, u_\phi) = \quad & \Big((-0.478u_\phi^3 - 3.06u_\phi^2 + 1.55u_\phi - 0.183)J_T^3 \\
& +(2.68u_\phi^3 + 5.13u_\phi^2 - 2.92u_\phi + 0.355)J_T^2 \\
& +(-3.15u_\phi^3 - 2.61u_\phi^2 + 1.78u_\phi - 0.226)J_T \\
& +(1.05u_\phi^3 + 0.361u_\phi^2 - 0.352u_\phi + 0.0472)\Big) \times 10^6 \\
K_{fp}(J_T, u_\phi) = \quad & \Big((-3.73u_\phi^3 + 0.602u_\phi^2 + 0.301u_\phi - 0.0487)J_T^3 \\
& +(8.76u_\phi^3 - 1.97u_\phi^2 - 0.453u_\phi + 0.0877)J_T^2 \\
& +(-6.82u_\phi^3 + 1.91u_\phi^2 + 0.180u_\phi - 0.0501)J_T \\
& +(1.77u_\phi^3 - 0.581u_\phi^2 - 0.00728u_\phi + 0.00882)\Big) \times 10^6.
\end{aligned}$$

Fig. 3 shows a comparison between $K^*_{rc_i}(J_T)$ in (13a) and $K_{rc}(J_T, u_\phi)$ in (14). The NRMSE is 5.03%. Fig. 3 shows a comparison between $K^*_{fp_i}(J_T)$ in (13b) and $K_{fp}(J_T, u_\phi)$ in (14). The NRMSE is 5.20%.

4.4. Mill States and Discharge Rate Constant

The initial state $\mathbf{x}^* = \left[x_w^*, x_s^*, x_r^*, x_f^*\right]^T$ in (1) is unknown. For industrial mills, the states inside the mill are not measured (Le Roux et al., 2017) and only reasonable assumptions can be made. In order to simulate the model, an initial state is required. Given a specific operating condition (J_T,u_ϕ), the initial states $\mathbf{x}^*$ can be calculated as follows:

1. Choose a value of d_q. A high d_q generally results in a high x_r^* and a low x_s^*, and vice versa.
2. Use (9b), (11) and $\beta_{ws} = \frac{x_w}{x_s} = 0.9$ to calculate: $x_s^* = \frac{(\beta_{ws}+1)Y_{Q_{S_i}}(J_T)}{d_q \beta_{ws} \varphi}$.
3. Calculate: $x_w^* = \beta_{ws} x_s^*$.
4. Use (2) to calculate: $x_r^* = v_{mill} J_T - x_b - x_s^* - x_w^*$.
5. Use (8) and (11) to calculate: $x_f^* = Y_{\psi_i}(J_T) x_s^*$.
6. Evaluate the ratio: x_r^*/x_s^*. If the ratio is too high or too low, choose a different d_q and return to the first step.

In this study, a desired ratio $x_r^*/x_s^* = 1.5$ was chosen for the three operating conditions $k = 1, 2, 3$ in Table 4. Based on the steps above, $d_q < 0$ was estimated for all three conditions as:

$$d_q = \arg\min_{d_q} \sum_{k}^{3} \left\| \frac{\left(\frac{x_r^*}{x_s^*}\right)_k - 1.5}{\max\left(\frac{x_r^*}{x_s^*}\right)_k} \right\|_2. \tag{16}$$

The result is $d_q = 36.4$ h^{-1} and the NRMSE for the minimization is 3.57%.

5. Simulations and Results

The aim of this section is to show that the model (10) produces realistic dynamic responses to input changes, and that it settles at the steady-states defined by the grind curves. Therefore, there are two simulation experiments:

1. Dynamic response to steps in u_w, u_o and u_ϕ.

Table 4: Evaluation of three steady-state operating conditions for $d_q = 36.4$ h^{-1}.

Operating condition 1: $(J_T, u_\phi) = (0.26, 0.65)$	
Initial conditions	$\mathbf{x}^* = \begin{bmatrix} 9.42 \\ 10.5 \\ 17.7 \\ 7.16 \end{bmatrix}$; $\mathbf{u}^* = \begin{bmatrix} 82.6 \\ 248 \\ 0.65 \end{bmatrix}$; $\mathbf{y}^* = \begin{bmatrix} 0.26 \\ 2950 \\ 91.7 \\ 0.684 \end{bmatrix}$
Process matrices	$\mathbf{A} = \begin{bmatrix} -25.9 & 15.4 & 0 & 0 \\ -19.1 & 8.35 & -0.0283 & 0 \\ 0.0283 & 0.0283 & 0.0283 & 0 \\ -12.4 & 12.3 & 0.599 & -8.77 \end{bmatrix}$; $\mathbf{B} = \begin{bmatrix} 1.00 & 0 & 0 \\ 0 & 0.187 & 199 \\ 0 & 0.183 & -199 \\ 0 & 0.0389 & 194 \end{bmatrix}$
Eigenvalues	$\Lambda = \text{diag}\{-8.77,\ -8.78 - 0.959i,\ -8.78 + 0.959i,\ 0.0279\}$
Eigenvectors	$\mathbf{T} = \begin{bmatrix} 0 & 0.239 + 0.402i & 0.239 - 0.402i & 0.00555 \\ 0 & 0.240 + 0.462i & 0.240 - 0.462i & 0.00933 \\ 0 & -0.00122 - 0.00291i & -0.00122 + 0.00291i & -0.998 \\ 1.00 & 0.715 & 0.715 & -0.0627 \end{bmatrix}$
Operating condition 2: $(J_T, u_\phi) = (0.30, 0.70)$	
Initial conditions	$\mathbf{x}^* = \begin{bmatrix} 12.4 \\ 13.8 \\ 19.8 \\ 9.20 \end{bmatrix}$; $\mathbf{u}^* = \begin{bmatrix} 109 \\ 326 \\ 0.70 \end{bmatrix}$; $\mathbf{y}^* = \begin{bmatrix} 0.30 \\ 3510 \\ 120 \\ 0.669 \end{bmatrix}$
Process matrices	$\mathbf{A} = \begin{bmatrix} -25.9 & 15.4 & 0 & 0 \\ -19.0 & 8.45 & 0.0810 & 0 \\ -0.0810 & -0.0810 & -0.0810 & 0 \\ -12.3 & 11.9 & 0.467 & -8.77 \end{bmatrix}$; $\mathbf{B} = \begin{bmatrix} 1.00 & 0 & 0 \\ 0 & 0.185 & 319 \\ 0 & 0.185 & -319 \\ 0 & 0.0365 & 126 \end{bmatrix}$
Eigenvalues	$\Lambda = \text{diag}\{-8.77,\ -10.4,\ -7.10,\ -0.0847\}$
Eigenvectors	$\mathbf{T} = \begin{bmatrix} 0 & -0.700 & 0.479 & 0.0173 \\ 0 & -0.706 & 0.584 & 0.0289 \\ 0 & -0.0111 & 0.0123 & 0.997 \\ 1.00 & -0.104 & 0.655 & 0.0689 \end{bmatrix}$
Operating condition 3: $(J_T, u_\phi) = (0.36, 0.75)$	
Initial conditions	$\mathbf{x}^* = \begin{bmatrix} 16.1 \\ 17.9 \\ 24.4 \\ 9.95 \end{bmatrix}$; $\mathbf{u}^* = \begin{bmatrix} 141 \\ 424 \\ 0.75 \end{bmatrix}$; $\mathbf{y}^* = \begin{bmatrix} 0.36 \\ 4020 \\ 156 \\ 0.556 \end{bmatrix}$
Process matrices	$\mathbf{A} = \begin{bmatrix} -25.9 & 15.4 & 0 & 0 \\ -19.1 & 8.31 & -0.0664 & 0 \\ 0.0664 & 0.0664 & 0.0664 & 0 \\ -10.9 & 9.25 & -0.286 & -8.77 \end{bmatrix}$; $\mathbf{B} = \begin{bmatrix} 1.00 & 0 & 0 \\ 0 & 0.185 & 814 \\ 0 & 0.185 & -814 \\ 0 & 0.0368 & 299 \end{bmatrix}$
Eigenvalues	$\Lambda = \text{diag}\{-8.77,\ -8.80 - 1.46i,\ -8.80 + 1.46i,\ 0.0641\}$
Eigenvectors	$\mathbf{T} = \begin{bmatrix} 0 & 0.598 - 0.0512i & 0.598 + 0.0512i & 0.0127 \\ 0 & 0.668 & 0.668 & 0.0213 \\ 0 & -0.00928 - 0.00115i & -0.00928 + 0.00115i & -0.999 \\ 1.00 & 0.385 + 0.214i & 0.385 - 0.214i & 0.0391 \end{bmatrix}$

2. Steady-state response to set point changes in J_T and steps in u_ϕ.

The model (10) is integrated using the explicit fourth-order Runge-Kutta method with a sampling time of 10 s. The parameters are obtained as described in Section 4. A constant value of $d_q = 35$ h^{-1} is used.

5.1. Dynamic Response

Three separate steady-state operating conditions as indicated in Table 4 are used to initialize the system and evaluate its dynamic response to steps in the inputs. There is no feedback controller to stabilize the outputs of the grinding mill. The model is linearized at each of the three initial states, and the dynamic response is evaluated based on the eigenvalues and eigenvectors for each operating condition.

5.1.1. Linearization, Eigenvalues and Eigenvectors

A brief overview of linear system theory is given below to support the eigenvalue analysis to follow. Readers familiar with linear system theory may glance over this section.

The non-linear model (10) is linearized at each steady-state condition $(\mathbf{x}^*, \mathbf{u}^*)$ as follows:

$$\dot{\tilde{\mathbf{x}}} = \mathbf{A}\tilde{\mathbf{x}} + \mathbf{B}\tilde{\mathbf{u}}, \tag{17}$$

where $\mathbf{A} = \frac{\partial \mathbf{f}}{\partial \mathbf{x}}|_{\mathbf{x}^*,\mathbf{u}^*}$, $\mathbf{B} = \frac{\partial \mathbf{f}}{\partial \mathbf{u}}|_{\mathbf{x}^*,\mathbf{u}^*}$, $\tilde{\mathbf{x}} = \mathbf{x} - \mathbf{x}^*$, and $\tilde{\mathbf{u}} = \mathbf{u} - \mathbf{u}^*$.

For this case $\mathbf{A}$ is a square 4×4 matrix. The eigenvalues λ_l and eigenvectors $\mathbf{t}_l$ $(l = 1, \ldots, 4)$ are the non-trivial solutions of:

$$(\mathbf{A} - \mathbf{I}\lambda_l)\,\mathbf{t}_l = 0 \quad \Leftrightarrow \quad \mathbf{A}\mathbf{t}_l = \lambda_l \mathbf{t}_l.$$

The eigenvalues λ_l are collected as diagonal elements in the matrix $\Lambda = \mathrm{diag}(\lambda_1, \ldots, \lambda_4^T)$ and the corresponding eigenvectors $\mathbf{t}_l$ as the columns in the matrix $\mathbf{T} = [\mathbf{t}_1, \ldots, \mathbf{t}_4]$. If the eigenvalues λ_l are mutually distinct, the eigenvectors $\mathbf{t}_l$ are linearly independent and a new state vector can be defined: $\mathbf{z} = \mathbf{T}^{-1}\tilde{\mathbf{x}} \Leftrightarrow \tilde{\mathbf{x}} = \mathbf{T}\mathbf{z}$. Therefore, the linearized system in (17) can be rewritten as:

$$\mathbf{T}\dot{\mathbf{z}} = \mathbf{A}\mathbf{T}\mathbf{z} + \mathbf{B}\tilde{\mathbf{u}} \quad \Leftrightarrow \quad \dot{\mathbf{z}} = \Lambda\mathbf{z} + \mathbf{T}^{-1}\mathbf{B}\tilde{\mathbf{u}}, \tag{18}$$

which is a set of decoupled differential equations in terms of the transformed states $\mathbf{z}$ (i.e., z_l is associated with the corresponding λ_l and $\mathbf{t}_l$). Since $\tilde{\mathbf{x}} = \mathbf{T}\mathbf{z}$, the eigenvector $\mathbf{t}_l$ indicates to what extent the corresponding eigenvalue λ_l influences each state in $\tilde{\mathbf{x}}$.

The unforced solution (i.e. $\tilde{\mathbf{u}} = \mathbf{0}$) for each state $\mathbf{z}$ in (18) is:

$$z_l(t) = z_l^* \exp(\lambda_l t),$$

where z_l^* is the initial value of $z_l(t)$. The eigenvalue λ_l indicates the rate at which the state decreases or increases exponentially over time. If the real part of λ_l is strictly smaller than zero the state is asymptotically stable ($z_l \to 0$ as $t \to \infty$). Otherwise the state is unstable ($z_l \to \infty$ as $t \to \infty$). Consequently, the linear system (17) is asymptotically stable if and only if all the real parts of the eigenvalues of $\mathbf{A}$ are strictly smaller than zero.

Therefore, although the eigenvalue analysis does not describe the global response of the non-linear system, it provides a valuable description of the response of the non-linear system within the local region where it was linearized (Skogestad and Postlethwaite, 2005).

5.1.2. Eigenvalue Analysis

Table 4 shows the operating condition in terms of J_T and u_ϕ, the initial states as obtained from Section 4.4, the linearized system matrices, as well as its eigenvalues and eigenvectors.

Compared to the data in Table 3, the first operating condition at $(J_T, u_\phi) = (0.26, 0.65)$ is such that J_T is above the point where the peak of Q_S is reached, but below the point where the peak of ψ is reached. The second operating condition at $(J_T, u_\phi) = (0.30, 0.70)$ is such that J_T is marginally below the point where the peak of Q_S is reached, and below the point where the peak of ψ is reached. The third operating condition

at $(J_T, u_\phi) = (0.36, 0.75)$ is at the highest speed and is marginally above the point where the peak of Q_S is reached, and above the point where the peak of ψ is reached.

As seen in Table 4, $\lambda_1 = -8.77$ for all three operating conditions. The corresponding eigenvector $\mathbf{t}_1 = [0,\ 0,\ 0,\ 1]^T$ indicates that λ_1 is associated exclusively with x_f. Similarly, eigenvectors $\mathbf{t}_2$ and $\mathbf{t}_3$ indicate that λ_2 and λ_3 are associated predominantly with the three states: x_w, x_s, and x_f. The eigenvalues λ_1, λ_2, and λ_3 are all stable and of similar magnitude. Therefore, the dynamic response of the states x_w, x_s, and x_f are stable and change at comparable rates.

The fourth eigenvalue λ_4 is associated predominantly with x_r. The magnitude of λ_4 is close to zero and implies that the state has a very slow integrating response. This integrating response is expected as x_r only enters the mill and does not discharge from the mill. The state x_r is stable for operating condition 2 ($\lambda_4 < 0$), but is unstable for operating conditions 1 and 3 ($\lambda_4 > 0$). As seen from the matrix entry A_{23} for operating conditions 1 and 3, an increase in x_r reduces x_s, i.e., x_r is not consumed rapidly enough to produce x_s and there is a slow unstable growth in x_r. Thus, the instability is related to the rate at which rocks are consumed compared to the total mass of rocks broken into solids. A general rule of thumb to ensure λ_4 is stable is to operate at a high u_ϕ where J_T is less than the value that maximizes Q_S (see Table 3).

5.1.3. Simulation Results

The normalized step changes in the inputs for the three operating conditions in Table 4 are shown in Fig 4. The normalized responses of the states are shown in Fig. 5, and the normalized responses of the outputs in Fig. 6. (The values are normalized with respect to the initial conditions given in Table 4 of the relevant operating condition.)

The states x_w, x_s, and x_f in Fig. 5 follow similar trends. As expected, the rates of change of these three states are comparable. As u_o reduces, x_s and x_f reduces, the slurry becomes more fluid and discharges from the mill quicker. The state x_r in Fig. 5 and the output J_T in Fig. 6 exhibit integrating behaviour for changes in u_o.

Changes in u_w do not produce similar responses as changes in u_o. When u_w increases, it causes the slurry in the mill to become fluid very quickly and effectively 'washes' x_s and x_f out of the mill. There is little to no effect on x_r as per definition the rocks are too large to discharge from the mill. The effect of u_w on J_T is a slight decrease which stabilizes fairly quickly. Finally, as expected, the movement of Q_S and ψ reflects the movement in u_o and x_f respectively.

As seen from $t = 14$ h to $t = 20$ h in Fig. 5 and 6, the step-change in u_ϕ in Fig. 4 has a strong non-linear effect on the operation of the mill. The decrease in u_ϕ causes a reduction in P_{mill}, which means that less energy is available to break ore. Because less ore is being broken, there is a rapid accumulation of rocks x_r

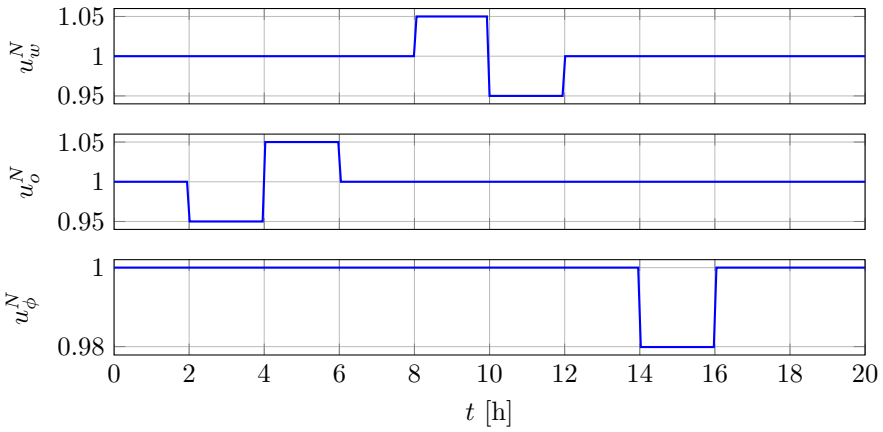

Figure 4: Open-loop step changes in manipulated variables. (The superscript N indicates that values are normalized according to the initial conditions shown in Table 4.)

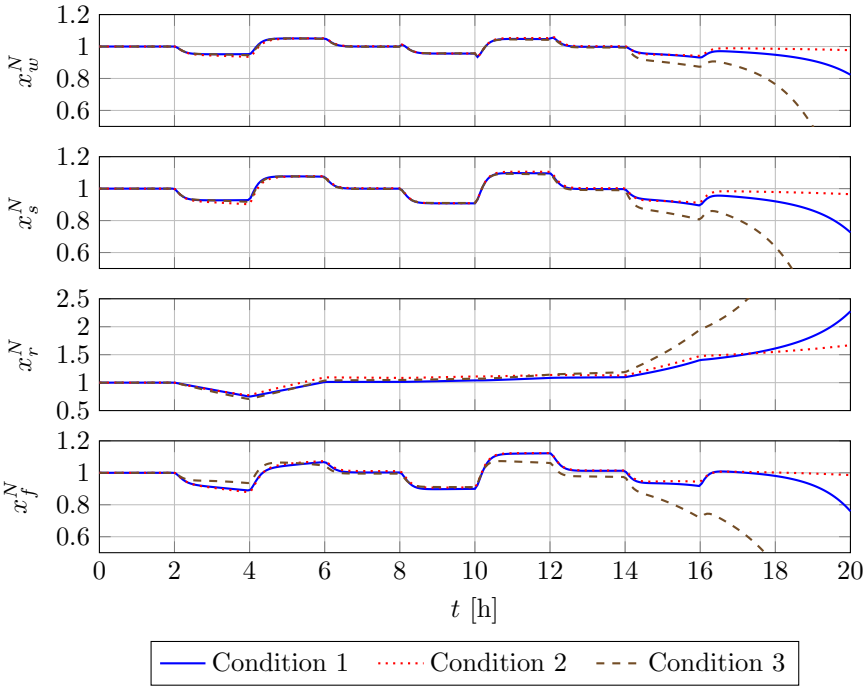

Figure 5: Dynamic response of the states for the three operating conditions according to Table 4. (The superscript N indicates that values are normalized according to the initial conditions shown in Table 4.)

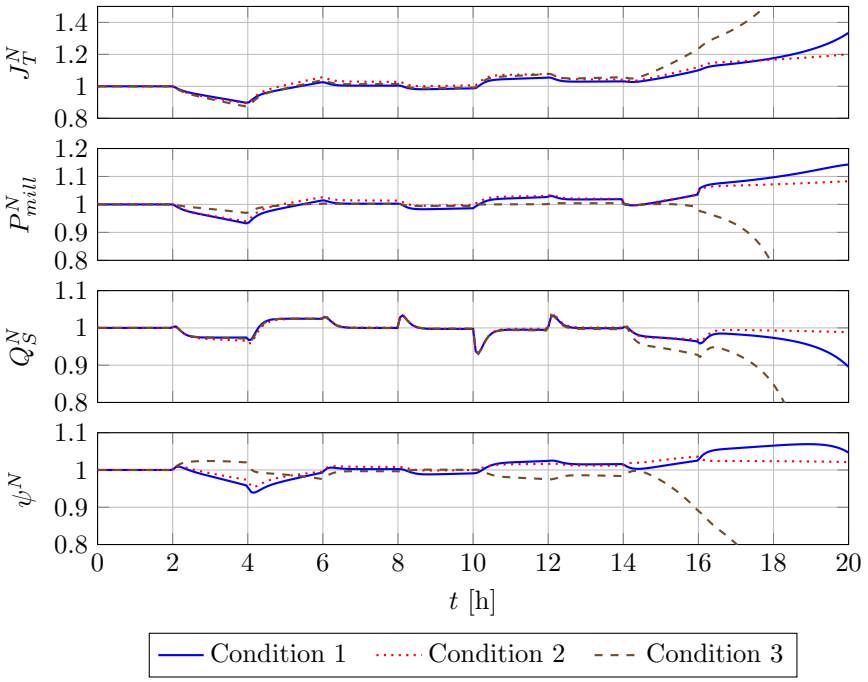

Figure 6: Dynamic response of the outputs for the three operating conditions according to Table 4. (The superscript N indicates that values are normalized according to the initial conditions shown in Table 4.)

and a subsequent increase in J_T. When u_ϕ returns to its nominal value at $t = 16$ h, J_T does not reduce accordingly since insufficient energy is applied to break the accumulated rocks x_r.

As seen in Fig. 6, the movement of ψ for Condition 3 is different to the other two conditions. Since the operating condition for Condition 3 is past the point where maximum ψ is reached in terms of J_T, it will respond in the opposite direction as the first two conditions. Similarly, since the operating condition for Condition 3 is so close to the peak of Q_S, it exhibits similar behaviour to the other two conditions.

Similar to a sump operating with a discharge pump, a mill acts as an integrator. Therefore, unless a feedback controller is applied to regulate J_T, the mill may become unstable for step-changes in input variables (Le Roux and Craig, 2019).

5.2. Steady-State Response

The mill is initialized at the second operating condition in Table 4. A series of set point changes to J_T and step changes to u_ϕ are made in order to recreate the full range of grind curve conditions. As mentioned above, a feedback controller is necessary to regulate changes in J_T. Therefore, a Proportional-Integral controller manipulates u_o to control J_T according to its set point. Since the grind curves assumed a constant ρ_Q, a Proportional controller manipulates u_w to maintain the ratio $\beta_{ws} = \frac{Q_W}{Q_S} = 0.9$.

Fig. 7 shows the response of the manipulated variables u_w and u_o, as well as the series of step changes to u_ϕ. Fig. 8 shows the controlled variable J_T and the controlled ratio $\beta_{ws} = \frac{Q_W}{Q_S}$. The response of the mill states are shown in Fig. 9. The output variables P_{mill}, Q_S, and ψ are shown in Fig. 10, where a data marker ($\circ$) is placed at the end of each set point change period to highlight an approximately steady-state condition. As expected, there is a large change in the output variables whenever there is a step change in u_ϕ. Note, x_r goes to 0 m^3 at approximately $t = 39$ h where J_T is very low and u_ϕ high.

Fig. 11 shows the data markers ($\circ$) of the output variables P_{mill}, Q_S, and ψ in Fig. 10 versus the data markers of J_T in Fig. 8. The original grind curves (11) are also shown in Fig. 11. The figure shows that the simulation model reproduces the steady-states as given by grind curves.

The system is linearized at each of the steady-state conditions indicated by the data markers ($\circ$) in Fig. 11. Similar to the analysis in Section 5.1.2, the eigenvalues for each of the linearized models are calculated and the results are plotted in Fig. 12. For $u_\phi = \{0.70,\ 0.75\}$, all eigenvalues are real and negative when J_T is

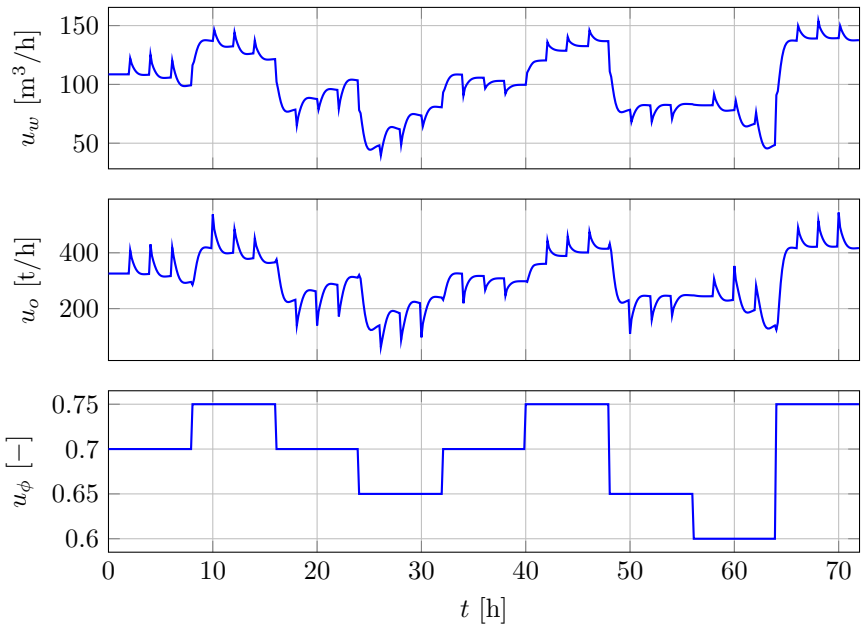

Figure 7: Manipulated variables for set point changes in J_T and step changes in u_ϕ.

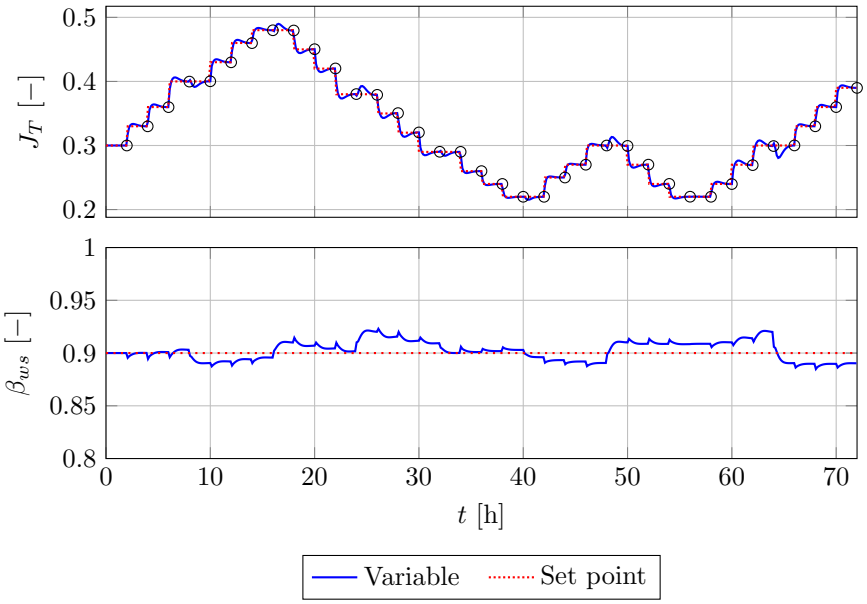

Figure 8: Controlled variables for set point changes in J_T and step changes in u_ϕ. The data markers (○) show the steady-state conditions and correspond to the data markers in Fig. 11.

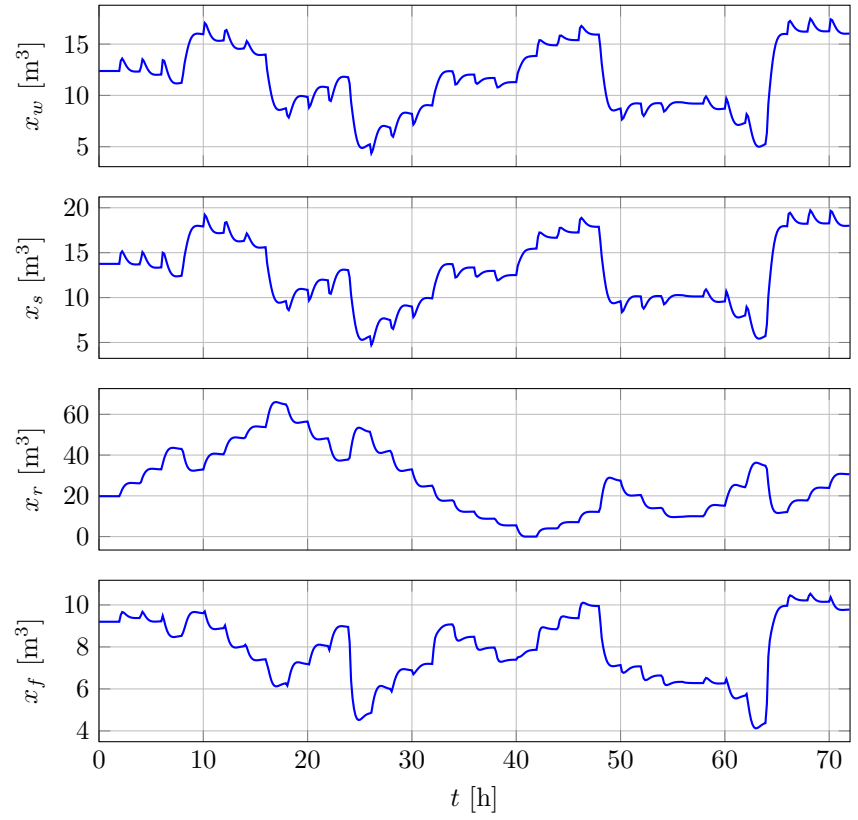

Figure 9: State response for set point changes in J_T and step changes in u_ϕ.

below the point where the maximum Q_S is achieved. When J_T surpasses this point, λ_2 and λ_3 form complex conjugate pairs and λ_4 becomes positive. Therefore, when the operating condition surpasses maximum throughput at high u_ϕ, there is an instability associated with x_r and oscillatory behaviour associated with

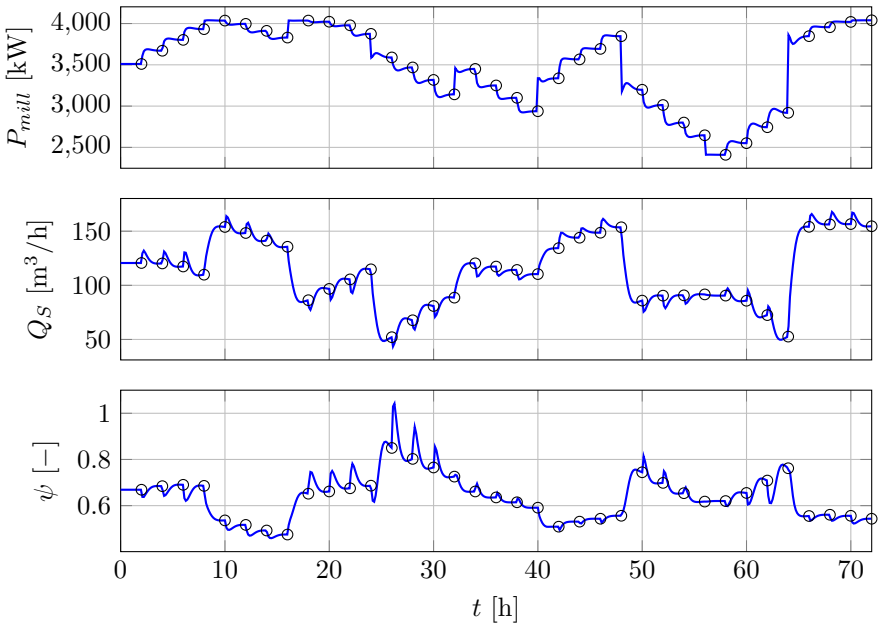

Figure 10: Measured variables for set point changes in J_T and step changes in u_ϕ. The data markers (∘) show the steady-state conditions and correspond to the data markers in Fig. 11.

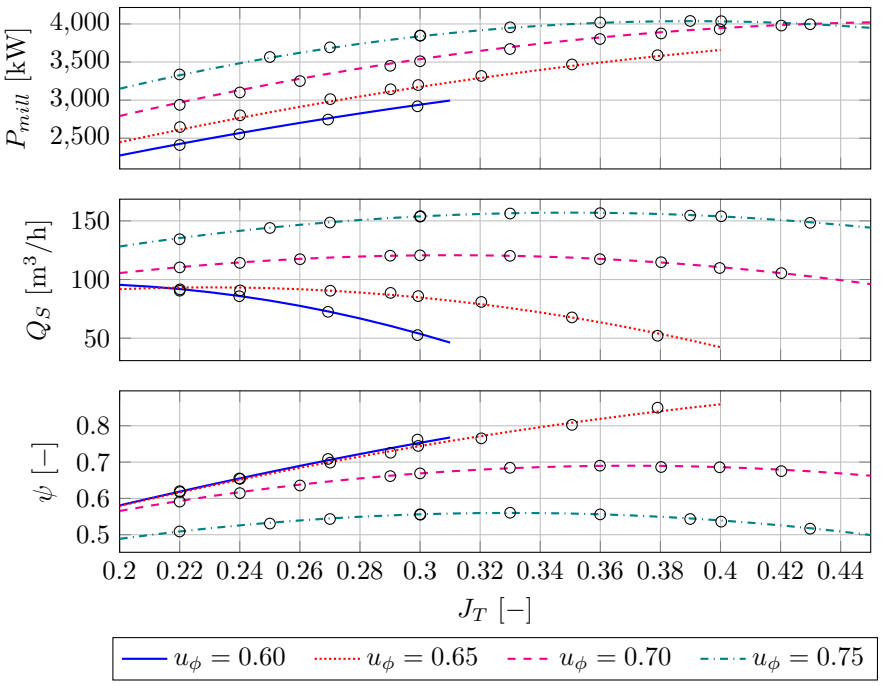

Figure 11: Map of steady-state data markers (∘) to original grind curves in Fig. 2.

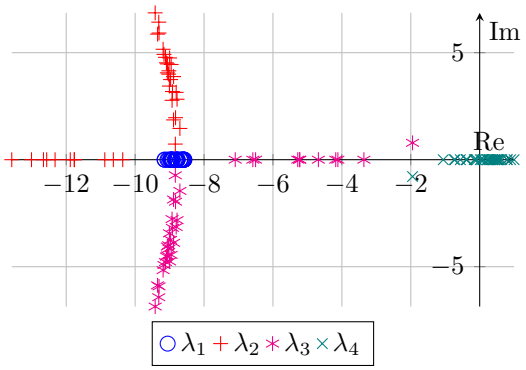

Figure 12: Plot of eigenvalues of system linearized at each steady-state indicated by the data markers (∘) in Fig. 11.

x_w and x_s. This agrees with the results in Table 4, where for Condition 3 there are complex conjugate pairs and one unstable eigenvalue when operating past the point where Q_S is a maximum, but where for Condition 2 there are real and stable eigenvalues when operating before the point where Q_S is a maximum in terms of J_T. However, the eigenvalues behave differently for the case where $u_\phi = \{0.60,\ 0.65\}$. When operating below this point for u_ϕ, eigenvalues λ_2 and λ_3 form complex conjugate pairs and λ_4 remains positive both above and below the point where Q_S is a maximum in terms of J_T. This confirms the general rule of thumb mentioned previously that the mill is stable for a relatively high u_ϕ where J_T is less than where the peak of Q_S is reached.

6. Conclusion

A dynamic non-linear model was fitted to the grind curve data of an industrial SAG mill by means of a step-wise procedure. The grind curves define the quasi-steady-state operation of the power draw, throughput, and grind of the mill in terms of the mill filling and mill rotational speed. Although only one data set was used, the procedure can be generalized for similar data sets. As seen in Section 5.1, the model produces realistic dynamic responses at each operating condition. As seen in Section 5.2, the model achieves the different steady-state conditions defined by the grind curves. Future work involves validating the model against time-series data measured while establishing the grind curves for an industrial grinding mill.

The non-linear model was linearized at three different steady-state operating conditions to evaluate the dynamic response of the model. The nature of the three linear models was analysed according to the eigenvalues and eigenvectors of the respective system matrices. The three linear models exhibit similar dynamics and capture the main trends of the model states. Depending on the operating condition, there may be an instability in terms of the volume of rocks in the mill. However, this is a slowly changing state and can be controlled with a simple feedback controller.

To evaluate the ability of the model to reach the various steady-state operating conditions defined by the grind curves, the model was simulated dynamically with step changes in the mill filling set point and the mill rotational speed. The mill was stabilized to steady-state for each step change with a simple feedback controller. Analysis of the performance variables - power draw, throughput, and grind - indicate that the model represents the range of quasi-steady-states given by the grind curves.

The model can be used for the development and analysis of supervisory and optimization control strategies which need to consider the full range of operating conditions and the associated dynamics of a grinding mill. For example, extremum seeking control (ESC) is an attractive control strategy to optimize the economic performance of the grinding mill (Krstíc and Wang, 2000). The advantage of ESC is that the controller can be agnostic to plant model as long as the economic performance index can be measured and has a peak. In practice such a control strategy implies that the expensive and difficult process to obtain the grind curves may not be necessary. The model presented in this paper was developed to simulate and test such a

control strategy. Future work involves the development of an ESC strategy to optimize the performance of a grinding mill.

Acknowledgement

This work is based on research supported in part by the National Research Foundation of South Africa (IRC grant number 111741).

Aguila-Camacho, N., le Roux, J. D., Duarte-Mermoud, M. A., Orcharda, M. E., 2017. Control of a grinding mill circuit using fractional order controllers. J. Process Control 53, 80–94.

Amestica, R., Gonzalez, G. D., Menacho, J., Barria, J., 1996. A mechanistic state equation model for semiautogenous mills. Int. J. Mineral Process. 44-45, 349–360.

Apelt, T. A., Asprey, S. P., Thornhill, N. F., 2002. Inferential measurement of SAG mill parameters II: State estimation. Minerals Eng. 15, 1043–1053.

Apelt, T. A., Thornhill, N. F., 2009. Inferential measurement of SAG mill parameters V: MPC simulation. Minerals Eng. 22, 1045–1052.

Chen, X., Zhai, J., Li, S., Li, Q., 2007. Application of model predictive control in ball mill grinding circuit. Minerals Eng. 20 (11), 1099–1108.

Coetzee, L. C., Craig, I. K., Kerrigan, E. C., 2010. Robust nonlinear model predictive control of a run-of-mine ore milling circuit. IEEE Trans. Control Syst. Technol. 18 (1), 222–229.

Craig, I. K., Hulbert, D. G., Metzner, G., Moult, S. P., 1992. Optimized multivariable control of an industrial run-of-mine milling circuit. J. S. Afr. Inst. Min. Metall. 92 (6), 169–176.

Craig, I. K., MacLeod, I. M., 1995. Specification framework for robust control of a run-of-mine ore milling circuit. Control Eng. Practice 3 (5), 621–630.

Craig, I. K., MacLeod, I. M., 1996. Robust controller design and implementation for a run-of-mine ore milling circuit. Control Eng. Practice 4 (1), 1–12.

Cramer, L. A., 2008. What is your PGM concentrate worth? In: Proc. 3rd Int. Platinum Conf. - Platinum in Transformation, SAIMM, Sun City, South Africa. pp. 387–394.

Gupta, A., Yan, D. S., 2006. Mineral Processing Design and Operation: An Introduction. Elsevier B. V., The Boulevard, Langford Lane, Kidlington, Oxford OX5 1GB, UK.

Hinde, A. L., Kalala, J. T., 2009. The application of a simplified approach to modelling tumbling mills, stirred media mills and HPGR's. Minerals Eng. 22 (7-8), 633–641.

Krstíc, M., Wang, H. H., 2000. Stability of extremum seeking feedback for general nonlinear dynamic systems. Automatica 36, 595–601.

Latchireddi, S., Morrell, S., 2003a. Slurry flow in mills: Grate-only discharge mechanism (Part-1). Minerals Eng. 16, 625–633.

Latchireddi, S., Morrell, S., 2003b. Slurry flow in mills: Grate-pulp lifter discharge systems (Part 2). Minerals Eng. 16, 635–642.

Le Roux, J., Craig, I. K., 2019. Plant-wide control framework for a grinding mill circuit. Ind. Eng. Chem. Res. 58, 11585–11600.

Le Roux, J. D., Craig, I. K., 2013. Reducing the number of size classes in a cumulative rates model used for process control of a grinding mill circuit. Powder Tech. 246, 169–181.

Le Roux, J. D., Craig, I. K., Hulbert, D. G., Hinde, A. L., 2013. Analysis and validation of a run-of-mine ore grinding mill circuit model for process control. Minerals Eng. 43-44, 121–134.

Le Roux, J. D., Olivier, L. E., Naidoo, M. A., Padhi, R., Craig, I. K., 2016. Throughput and product quality control for a grinding mill circuit using non-linear MPC. J. Process Control 42, 35–50.

Le Roux, J. D., Steinboeck, A., Kugi, A., Craig, I. K., 2017. An EKF observer to estimate semi-autogenous grinding mill hold-ups. J. Process Control 51, 2741.

McIvor, R., Finch, J., 1991. A guide to interfacing of plant grinding and flotation operations. Minerals Eng. 4 (1), 9–23.

Morrell, S., 2004. A new autogenous and semi-autogenous mill model for scale-up, design and optimisation. Minerals Eng. 17 (3), 437–445.

Nelder, J., Mead, R., 1965. A simplex method for function minimization. Comput. J. 7, 308313.

Olivier, L. E., Craig, I. K., 2013. Model-plant mismatch detection and model update for a run-of-mine ore milling circuit under model predictive control. J. Process Control 23 (2), 100–107.

Pomerleau, A., Hodouin, D., Desbiens, A., Gagnon, E., 2000. A survey of grinding circuit control methods: from decentralized PID controllers to multivariable predictive controllers. Powder Tech. 108 (2-3), 103–115.

Powell, M. S., Mainza, A. N., 2006. Extended grinding curves are essential to the comparison of milling performance. Minerals Eng. 19, 1487–1494.

Powell, M. S., Morrell, S., Latchireddi, S., 2001. Developments in the understanding of South-African style SAG mills. Minerals Eng. 14, 1143–1153.

Powell, M. S., Morrison, R. D., 2007. The future of comminution modelling. Int. J. Mineral Process. 84 (1-4), 228–239.

Powell, M. S., Perkins, T., Mainza, A. N., 2011. Grindcurves applied to a range of SAG and AG mills. In: Proc. SAG 2011, Vancouver, B.C., Canada.

Powell, M. S., van der Westhuizen, A. P., Mainza, A. N., 2009. Applying grindcurves to mill operation and optimisation. Minerals Eng. 22 (7-8), 625–632.

Salazar, J., Magne, L., Acua, G., Cubillos, F., 2009. Dynamic modelling and simulation of semi-autogenous mills. Minerals Eng. 22 (1), 70–77.

Salazar, J., Valdez-Gonzalres, H., Vyhmesiter, E., Cubillos, F., 2014. Model predictive control of semi-autogenous mills. Minerals Eng. 64, 92–96.
Sbarbaro, D., del Villar, R., 2010. Advanced Control and Supervision of Mineral Processing Plants. Springer-Verlag London Limited.
Skogestad, S., 2004. Control structure design for complete chemical plants. Computers Chem. Eng. 28, 219–234.
Skogestad, S., Postlethwaite, I., 2005. Multivariable Feedback Control: Analysis and Design, 2nd Edition. John Wiley & Sons Ltd.
Song, C., Wang, P., Makse, H. A., 2008. A phase diagram for jammed matter. Nature 453 (7195), 629632.
Sosa-Blanco, C., Hodouin, D., Bazin, C., Lara-Valenzuele, C., Salazar, J., 2000. Economic optimisation of a flotation plant through grinding circuit tuning. Minerals Eng. 13 (10-11), 999–1018.
Steyn, C. W., Sandrock, C., 2013. Benefits of optimisation and model predictive control on a fully autogenous mill with variable speed. Minerals Eng. 53, 113–123.
Tungpalan, K., Manlapig, E., Andrusiewicz, M., Keeney, L., Wightman, E., Edraki, M., 2015. An integrated approach of predicting metallurgical performance relating to variability in deposit characteristics. Minerals Eng. 71, 49–54.
Valery, W., Morrell, S., 1995. The development of a dynamic model for autogenous and semi-autogenous grinding. Minerals Eng. 8 (11), 1285–1297.
Van der Westhuizen, A. P. P., Powell, M. S., 2006. Milling curves as a tool for characterising SAG mill performance. In: Proc. SAG 2006, Vancouver, B.C., Canada. pp. 217–232.
Viklund, T., Albertsson, J., Burstedt, J., Isaksson, M., Soderlund, J., 2006. Evolution of AG mill control system at Boliden Mineral AB. In: Proc. SAG 2006, Vancouver, B.C., Canada. pp. 311–325.
Wakefield, B. J., Lindner, B. S., McCoy, J. T., Auret, L., 2018. Monitoring of a simulated milling circuit: Fault diagnosis and economic impact. Minerals Eng. 120, 132–151.
Wei, D., Craig, I. K., 2009. Grinding mill circuits - A survey of control and economic concerns. Int. J. Mineral Process. 90 (1-4), 56–66.